Gas-phase photocatalytic decomposition of ethylbenzene over perlite granules coated with indium doped TiO2

Article *in* The Chemical Engineering Journal · May 2013

DOI: 10.1016/j.cej.2013.01.066

CITATIONS
15

READS
134

4 authors:

Mariana Hinojosa Reyes
Instituto Potosino de Investigación Científica …
6 PUBLICATIONS **51** CITATIONS
SEE PROFILE

Sonia Arriaga
Instituto Potosino de Investigación Científica…
35 PUBLICATIONS **626** CITATIONS
SEE PROFILE

Luis Armando Diaz-Torres
Centro de Investigaciones en Optica
110 PUBLICATIONS **1,324** CITATIONS
SEE PROFILE

Vic Rdz Glez
Instituto Potosino de Investigación Científica…
64 PUBLICATIONS **544** CITATIONS
SEE PROFILE

Chemical Engineering Journal 224 (2013) 106–113

Contents lists available at SciVerse ScienceDirect

Chemical Engineering Journal

journal homepage: www.elsevier.com/locate/cej

Gas-phase photocatalytic decomposition of ethylbenzene over perlite granules coated with indium doped TiO_2

M. Hinojosa-Reyes [a], S. Arriaga [b], L.A. Diaz-Torres [c], V. Rodríguez-González [a,*]

[a] División de Materiales Avanzados, IPICYT, Instituto Potosino de Investigación Científica y Tecnológica, Camino a la Presa San José 2055, Lomas 4a. sección C.P. 78216, San Luis Potosí, S.L.P., México
[b] División de Ciencias Ambientales, IPICYT, Instituto Potosino de Investigación Científica y Tecnológica, Camino a la Presa San José 2055 Lomas 4a. sección C.P. 78216, San Luis Potosí, S.L.P., México
[c] Grupo de Espectroscopia de Materiales Avanzados y Nanoestructurados (EMANA), Centro de Investigaciones en Óptica, A. C., Loma del Bosque 115, Lomas del Campestre, C.P. 37150 León, Gto., Mexico

HIGHLIGHTS

- The In–TiO_2 was coated on silicate granules for gas-phase ethylbenzene degradation.
- Plug-flow reactor packed with In–TiO_2/granules was used to evaluate the degradation.
- In–TiO_2 coated/granules show an enhanced decomposition rate of ethylbenzene.
- Photodecomposition rate of ethylbenzene strongly depends on the % of In_2O_3 into TiO_2.
- In_2O_3–TiO_2/perlite composites may be a practical way to decompose VOCs in moist gas.

GRAPHICAL ABSTRACT

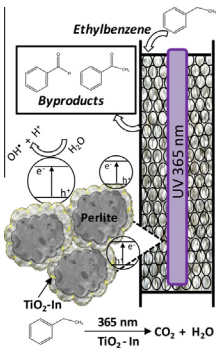

ARTICLE INFO

Article history:
Available online 29 January 2013

Keywords:
VOCs
BTEX
In-doped TiO_2/perlite
Ethylbenzene
Gas phase photo-oxidation

ABSTRACT

Doped indium–TiO_2 mesoporous photocatalysts were synthesized by a controlled sol–gel process. The catalysts were characterized by XRD, N_2 physisorption, UV–Vis-DRS, Photoluminescence and Raman spectroscopies. The indium–TiO_2 semiconductors were immobilized on perlite granules by a simple coating method and examined by SEM-EDS. Photocatalytic activity of the In–TiO_2/perlite materials was evaluated by the decomposition of ethylbenzene in moist air in a plug-flow photoreactor with a concentric cylindrical configuration, under 254 or 365 nm irradiation. Ethylbenzene was substantially decomposed by oxidation in an air steam flowing over the In-doped coated/perlite granules. The decomposition rate of ethylbenzene may be attributed to the presence of indium, which can increase surface phenomena and sensitize the response of the semiconductors to the 365 nm UV irradiation. The materials with indium content show enhanced decomposition rates in contrast to the undoped materials. The study indicates that the immobilized In–TiO_2/perlite photocatalysts may be a practical way to decompose volatile organic compounds in a stream of moist gas.

1. Introduction

The quality of indoor air has a direct effect on human health in terms of prolonged exposure to pollutants by inhalation of Volatile Organic Compounds (VOCs). VOCs, are components of materials like paints and varnishes, pesticides, building materials and furnishings, office equipment such as copiers and printers [1]. Some of them have short- and long-term adverse health effects. Concentrations of many VOCs are consistently higher indoors than outdoors and are the major pollutants of indoor air [2,3]. Ethylbenzene (EB) is emitted to the atmosphere in practically all

* Corresponding author. Tel.: +52 444 834 2000x7295; fax: +52 444 834 2010.
E-mail address: vicente.rdz@ipicyt.edu.mx (V. Rodríguez-González).

1385-8947/$ - see front matter © 2013 Elsevier B.V. All rights reserved.
http://dx.doi.org/10.1016/j.cej.2013.01.066

combustion processes, including all point and mobile combustion sources that utilize fossil fuels [3]. In indoor environments, EB exposure occurs predominantly from the use of certain consumer products, solvents, carpet glues, varnishes, paints, and tobacco smoke [3]. EB is, therefore, ubiquitous in outdoor and indoor urban and rural air.

Photocatalytic processes have been used to decompose benzene, toluene, ethylbenzene, and xylenes, BTEX compounds in aqueous medium [4,5] and gas phase systems [6,7]. Commercial TiO_2 and TiO_2-doped catalysts show promising results in removing these BTEX compounds [7–9]. Some photocatalysts have been immobilized for use in UV reactors, supported on activated carbon and silicates, such as perlite, as practical effective systems [10,11]. Typical TiO_2 P25 dispersions on cement paste show three to ten times less gas phase BTEX photodegradation activity that blank P25 in a mixed flow annular reactor. The photocatalytic activity is linearly dependent on the concentration of contaminant and the irradiation range [12]. The photocatalytic removal of EB was studied in-vehicle air with relative humidity 70–80%, in which the commercial TiO_2 was used to coat the inside of a glass tube. The destruction of EB at concentrations associated with in-vehicle air quality is closely 100%. The decomposition of EB appears to be independent of the relative humidity, but related to gas flow time [13]. Perlite is normally composed of aluminosilicates, and has a porous structure that gives it unique characteristics as a support of active materials [14]. Porous materials like perlite have surface roughness and also low density (approximately 0.41–0.44 g cm^{-3}), a relatively light weight material, so good material for packing cylindrical reactor without increase the total weight of the system. Normally, the roughness surface of perlite is partially hydroxylated and allows the formation of a homogenous coating on the surface. The applications of the perlite are principally the adsorption of dyes [15,16] and to coated photocatalytic materials for decomposition of contaminants [17,18].

The effect of water in the photo-oxidation of BTEX compounds in the gas phase was studied in an annular reactor operated in the continuous stirred-tank reactor (CSTR). The TiO_2 was coated onto the internal coaxial glass surface by dip coating method [19]. In absence of water EB was more difficult to oxidize than benzene and toluene, but easier than m-xylene. In presence of water, EB becomes the most readily oxidized compound. CO_2 was detected as the only product during photo-oxidation [19]. Ln^{3+}–TiO_2 semiconductors coated on a glass microfiber filter showed enhance photocatalytic degradation of EB in the continuous gas flow reactor. Materials with a lanthanide ion doping of 1.2% had the highest photoactivity. In this case the improved adsorption capacity of the doped-TiO_2 and electron–hole pairs separation seems to be responsible of the photodegradation. These titania doped materials decline in activity in a high humidity environment [6]. When indium cations was doping into the TiO_2 framework, the materials show enhanced photoxidation of 2,4-D under UV irradiation, in contrast to P25 impregnated with In_2O_3 particles [20]. Also indium incorporation increases the photoactivity under visible irradiation for the decomposition of Orange dye and sulfur mustard [21]. In the literature, there are only photocatalytic applications in aqueous medium or for inactivation of *Psedomonas fluorescens* and *Lactococcus lactis*, indium doped materials show enhanced activity that impregnated or commercial TiO_2 [22–24]. In the present research, for the first time, we want to study the effect of indium doped TiO_2 for the gaseous EB photoxidation. Highly-dispersed indium–TiO_2 particles were coated on perlite granules. A plug-flow gas phase photo-reactor, concentrically packed with TiO_2–In/perlite materials was used to evaluate EB decomposition rate in moist air of In–Ti/perlite coatings and the associated reaction rate constant (k/m^2) were determined. A discussion of the role of surface physicochemical properties of the immobilized In–TiO_2 on the photo-oxidation of EB is also presented.

2. Experimental section

2.1. Indium-doped TiO_2 sol–gel synthesis

Indium-doped TiO_2 sol–gel photocatalysts were prepared by a controlled hydrolysis sol–gel process using titanium (IV) isopropoxide (Sigma–Aldrich 97%) and indium (III) acetylacetonate (Aldrich 99.99%) as precursors [20,25]. First an appropriated amount of indium acetylacetonate to obtain 1.0 and 5.0 wt% In, was dissolved in acetone and placed in an ultrasonic bath for 5 min to assure the complete disaggregation of the indium precursor, Table S1 (see Supplementary section). The In–TiO_2 nanocomposite was prepared by adding dropwise 93.58 mL of titanium isopropoxide, 42.6 mL n-butanol (Sigma–Aldrich 99.8%) and the indium solution to a 42.6 mL n-butanol–22.4 mL water solution contained in a 4-neck round bottom flask (1 L) equipped with magnetic stirrer and thermometer. The alkoxide/n-butanol/water molar ratio was 1/3/8. Then, the solution was vigorously stirred at 50 °C until all the reagents were added (see Table S1 supplementary). Then, the solution was gradually heated to 70 °C. The gelled product was aged for 24 h at 70 °C. The solvents and unreacted precursors were removed in a vacuum evaporator at 80 °C, dried overnight under vacuum at 100 °C. Then materials were thermally treated at 400 °C for 4 h at a rate of 2 °C min^{-1}.

2.2. Immobilization of sol–gel In–TiO_2 on perlite granules

The perlite granules were impregnated with the In–TiO_2 catalysts according to the methodology reported by Hosseini et al. [10]. In brief, a slurry was prepared with 10 g of In–TiO_2 powder in 150 mL of ethanol, and the pH was adjusted at 3.5 using hydrochloric acid solution, 0.5 N. Then completely dispersed using an ultrasound bath for 15 min. The coating of photocatalyst over the perlite granules (45 g) was performed by adsorption of the slurry during 60 min of gentle mixing of the granules in the slurry. Then the solution evaporated at 80 °C. Finally, the granules were stabilized at 450 °C for 0.5 h and then washed twice with distilled water. The coated samples were identified as Ti-0/perlite, In–Ti-1/perlite and In–Ti-5/perlite, where 1 and 5 denote different indium content in wt%.

2.3. Characterization of photocatalysts

The specific surface areas were calculated from the nitrogen adsorption isotherms by the BET method using a Micrometrics ASAP 2020 apparatus. The TiO_2 crystalline phase and crystallite size were determined by X-ray diffraction with a Bruker Advance 8 Diffractometer with Cu Kα radiation (1.5404 Å). The UV–Vis spectra of solids were obtained with a Shimadzu Spectrometer model UV-2401 PC (diffuse reflectance mode). The band gap of the solids was calculated by linearization of the slope to the *X* axis (wavelength, nm) with the *Y* axis (absorbance) equal to zero. The morphology of coated perlite granules were characterized by a Field emission scanning electron microscopy (FE-SEM), Phillips XL 30S FEG. The coated perlite was analyzed by energy dispersive X-ray spectroscopy (EDS) detector coupled to the FE-SEM unit. Photoluminescence characterization measurements were performed at room temperature on an Acton Research modular 2300 spectrofluorometer. The excitation source was a 50 W Xe CW lamp tuned by an Acton Spectra Pro 300i at 350 nm. Emission was collected through a 400 nm long pass filter (rejection limit 375 nm, OD > 2) and then analyzed with an Acton Spectra Pro 500i monochromator and a R955 Hamamatsu photomultiplier, connected to an Acton Research Spectra HUB.

2.4. Photocatalytic decomposition of ethylbenzene

The experimental plug-flow reactor set-up designed for the photocatalytic evaluation is shown in Fig. 1. The photocatalytic EB decomposition in the gas phase was performed in a reactor with a volume of 153 mL at room temperature. The photoreactor consists of two concentric tubes. The inner quartz tube has a low-pressure mercury pen ray lamp which operates at 254 nm and 4400 μW cm^{-2} or 365 nm and 145 μW cm^{-2} (UVP products). Typical intensity for these lamps is effective at 1″ outer distance. The outer Pyrex tube was packed with ~23 g of previously In–TiO_2 impregnated granular perlite (3 × 3 × 7 mm) and perlite uncoated as a control. The coated perlite was washed with water before being packed in the photoreactor to confirm the stability of the coated film showing a negligible lixiviation of the coating.

Initially, we take samples in both valves sampling until is confirmed the stability of the flow, which means same flows for the in and out valves, Fig. 1. Once the stability is confirmed the light was turned on, and the kinetics were monitored. The kinetic parameters were monitored by collecting samples only from the out valve. All the kinetic parameters were determined at steady state.

The composition of the gas phase (containing EB and water) was analyzed by injecting 100 μL gas samples into a 6890 series gas chromatograph – FID (Agilent Technologies) with a capillary column (DB-624). The initial concentration of EB was 1.5 gm^{-3} (345.5 ppmv) at a relative humidity of 60% The photocatalytic experiments were repeated three times with a reproducibility of better than 5%. Prior to catalytic test reactions, a flow of moist EB was passed through the packed reactor for 3 h in order to achieve adsorption–desorption equilibrium, since water adsorbed onto TiO_2/perlite surfaces becomes a source of hydroxyls radicals.

3. Results and discussion

3.1. Crystalline phase, textural and optical properties

The specific surface areas for the materials Ti-0, In–Ti-1, In–Ti-5 and P25 are reported in Table 1. High specific surface areas (96–112 m^2g^{-1}) for all of the In–TiO_2 nanocomposites were obtained. The highest BET surface area is observed with the In–Ti-5 photocatalyst. The BET surface specific area increases with the indium content in the sample. The enhanced specific surface area in the sol–gel In–TiO_2 semiconductors may be the result of the method of synthesis and the co-gelling of titanium alkoxide with indium (III) acetylacetonate under controlled hydrolysis conditions for In–TiO_2. The results agreed well with our previous works [20,25] as well as with TiO_2 doped sol–gel results found in the literature [26,27].

The XRD patterns obtained for the Ti-0, In–Ti-1, In–Ti-5 and P25 samples, Fig. 2a, indicate the formation of anatase as the main crystalline TiO_2 phase (JCPDS 21-1272). The XRD pattern of commercial TiO_2 P25 also shows peaks attributable to the rutile TiO_2 crystalline phase (JCPDS-89-4920). Peaks attributable to indium particles (In^0 or In_xO_y) were not detected, even with the samples containing 5 wt% of Indium incorporated [28,29]. Therefore, it is assumed that some In^{3+} ions may have been inserted into the TiO_2 framework or deposited as nanometer-sized particles on the TiO_2 surface, which are not detectable by XRD. By using the Debye–Scherer equation, the crystallite size was calculated from the full width at half-maximum (FWHM) of the (1 0 1) anatase peak at 25.2° of 2θ. The results are presented in Table 1. At higher indium content, smaller crystallites are obtained (~8 nm), that suggests that doping of TiO_2 with In^{3+} ions may retard crystal growth. The smaller crystallites may lead to greater surface area with modified TiO_2 oxides and probably most of the indium incorporation will be on the surfaces of the crystallites. Similar crystallite size has been reported for TiO_2 doped with indium [26]. In addition, the crystallite size was smaller for higher indium content. The electronic configuration and the ionic radii of indium, titanium, and oxygen are $[Kr]4d^{10}5s^25p^1$, $[Ar]3d^24s^2$, $[He]2s^22p^4$, and 1.04, 0.96, 0.22 Å [21], respectively. If some In^{3+} ions replace some Ti^{4+} ions or some superficial O^{2-} ions in these structures, the TiO_2 framework will be stressed, which may constrain the growth of TiO_2 anatase crystallites, thereby affecting the O—Ti—OH surface bonds. According to the cited ionic radii it is most probably that O^{2-} ions stressed the framework and constrain the growth of TiO_2 anatase crystallites, then probably indium ions replace some Ti^{4+} ions. This hypothesis is in accordance with textural analysis, and XRD results that agree well with the

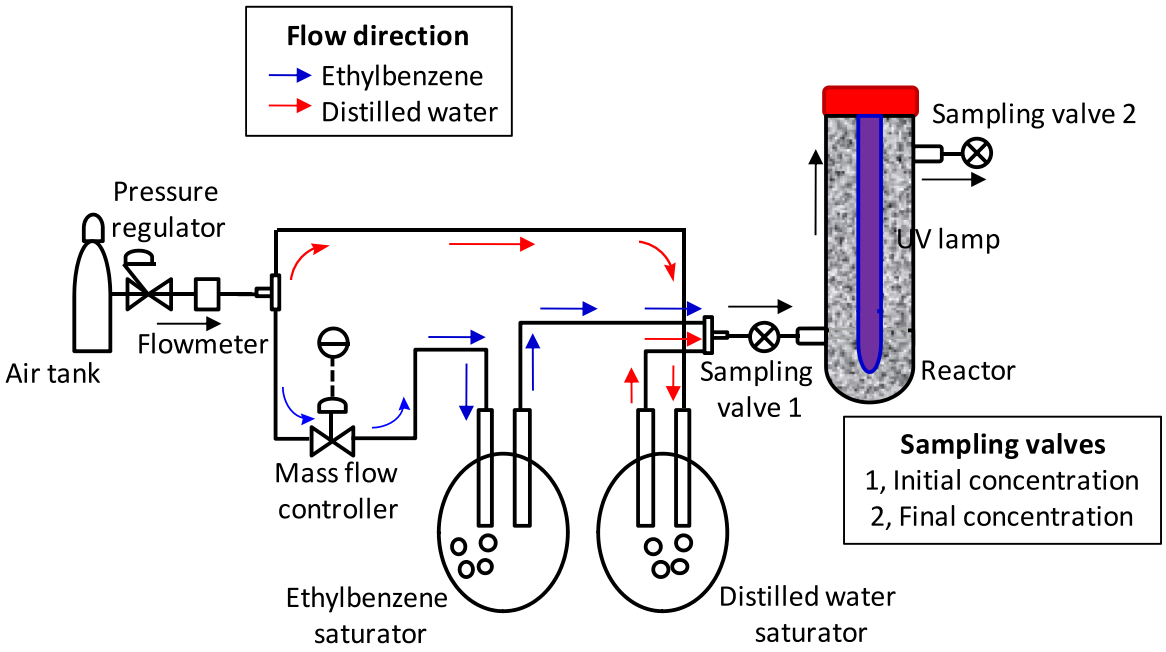

Fig. 1. The experimental reactor set-up designed for the photocatalytic ethylbenzene degradation.

Table 1
Physical properties of TiO_2 catalysts.

	Eg (eV)	Crystallite size (nm)	S_{BET}[a] $m^2 g^{-1}$
P25	3.26	19.60	52.02
Ti-0	3.27	11.90	73.52
In–Ti-1	3.24	8.39	95.56
In–Ti-5	3.32	8.16	112.35

[a] Specific superficial area.

results reported by Chen et al. [26] and with our previous observations [20,25]. The samples In–Ti-1 and In–Ti-5 were sintered at 1000 °C in order to segregate In_2O_3 doped or growth of particles dispersed on surface. The XRD pattern shows peaks assignable to In_2O_3 (JCPDS 6-0416) anatase and rutile TiO_2 phases (see Fig. 2b). Apparently, at such annealing temperature, In_2O_3 was formed. The thermal stability that indium provides to titania preserving 85.4% of anatase phase at 800 °C seems remarkable. Fig. 2b.

Raman characterization was carried out in doped materials in order to detect changes in the bonding of the framework of TiO_2. Fig. 3a, shows the Raman spectra of the indium doped and undoped materials. At 400 °C no changes in the characteristic Raman modes of TiO_2 were detected due to indium incorporation. However, at 1000 °C the dominant Raman modes are attributables to the anatase and rutile TiO_2 crystalline phases, Fig. 3b. From the XRD and Raman results, the 5% of indium oxide incorporated is appropriated for obtained In^{3+} doping or highly dispersed on TiO_2 crystallite surface. Higher concentration of In^{3+} (10%), was reported to produce stress in the TiO_2 framework show by changes in the Raman spectra [20,27].

From the UV–vis diffuse reflectance spectra of In–TiO_2 and P25 materials, the absorption edge (325–350 nm) has shifted slightly to longer wavelengths with the incorporation of 5%wt. indium in the nanocrystalline In–Ti-5 material. The estimated band-gap energy (Eg) is shifted from 3.27 eV (In–Ti-0) to 3.32 eV, (see Table 1). The increase in the band-gap energy is correlated with the indium oxide band-gap of 3.7 eV [29]. In addition, some vacancies due to In^{3+} incorporation into the TiO_2 framework may shift the band-gap energy. Such shift of the Eg absorption has also been reported for indium impregnated into TiO_2 sol–gel substrates [20,30]. The band-gap results may support the assumption of the incorporation of nanometric indium particles on the TiO_2 surface or the replacement of some Ti^{4+} and/or O^{2-} superficial ions [20,27]. In indium nanoparticles prepared by a similar method on nanocrystalline TiO_2, the Eg shift was also observed [20,26,27]. In the present study, it is assumed that the enhanced specific surface area of the incorporated indium nanoparticles in crystalline sol–gel TiO_2 (96–112 $m^2 g^{-1}$) allows for the formation of UV semiconductors, which may be excited by the absorption of UV irradiation. These semiconductors are UV sensitized by incorporation In_2O_3 in the gelling step of sol–gel synthesis and thermal stabilized.

3.2. SEM analysis of coated indium–TiO_2 /perlite composites

The SEM images show the morphology due to the coated process: island structures formed in raised agglomeration (Fig. 4a–e), with similar morphology for all TiO_2 deposition conditions, both indium doped and undoped. When the immobilization of In–TiO_2 is carried out in aqueous media under acidic conditions, several interconnected aggregates with faceted-grains are observed. Changes or decreases of crystallite size in indium doped TiO_2 due to the coating process, as show in these figures. The FE-SEM images, as well as the EDS analysis, confirm that homogenous coating of TiO_2 and In–TiO_2 results after 60 min. The EDS spectra of In–Ti-1/perlite show the TiO_2 composition and also the aluminosilicate composition of the granules of perlite, Fig. 4a. Other work has indicated that the sonochemical method can also lead to the coating of TiO_2 doped sol–gel in aluminosilicate materials with similar coverage [14].

3.3. Photocatalytic decomposition of ethylenbenzene

The photocatalytic activity of the EB decomposition in gas phase, at pressure and ambient temperature, was determined for all of these photocatalysts. The percentage of decomposition (D) was calculated at steady state. First under UV 365 nm. The corresponding % D, the decomposition rates (DR) and velocity constants are reported in Table 2. All of the photocatalysts show more activity than direct photolysis (3.3%). It can be seen that In–Ti-5/perlite sample show the highest D (23.3%) and the highest DR (1.8 mol $g^{-1}s^{-1}$). For the catalysts with In–Ti-1/perlite granules, the % D is 21.9, which is 1.78 times that of the % D of the undoped Ti-0/perlite photocatalyst. The performance of P25/perlite is lower than that observed for the Indium doped/perlite catalysts.

The photolysis with 254 UV irradiation was 1.64 times higher than in black at UV irradiation 365 nm. This means that the doped species show a higher photocatalytic DR, which we suspect may be due to UVA may photosensitize the In-doped TiO_2 materials, Fig. S2 and Table S2. At 254 nm UV irradadiation the remarkable behavior

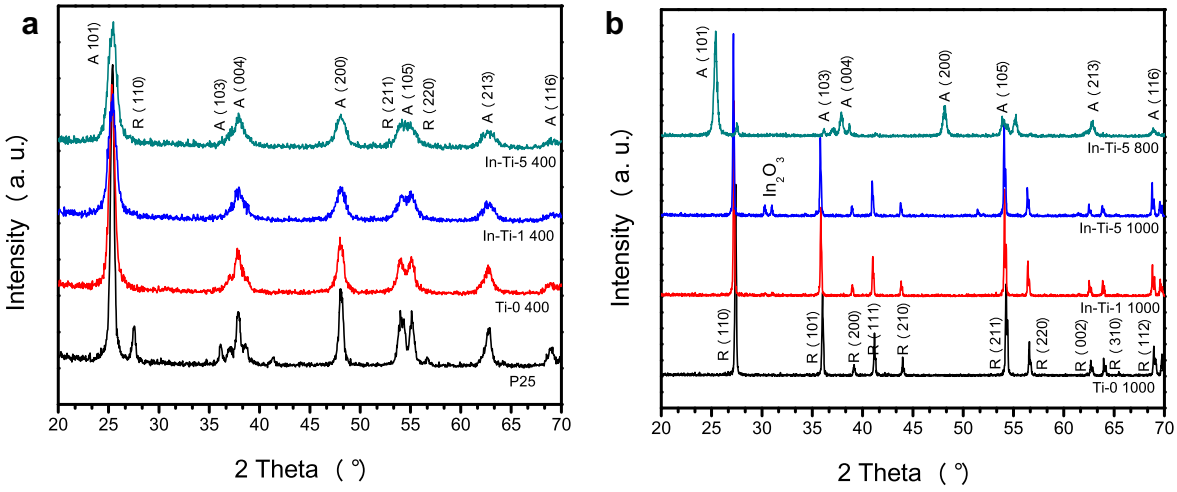

Fig. 2. XRD patterns of sol–gel semiconductors calcined: (a) at 400 °C (b) at 1000 °C.

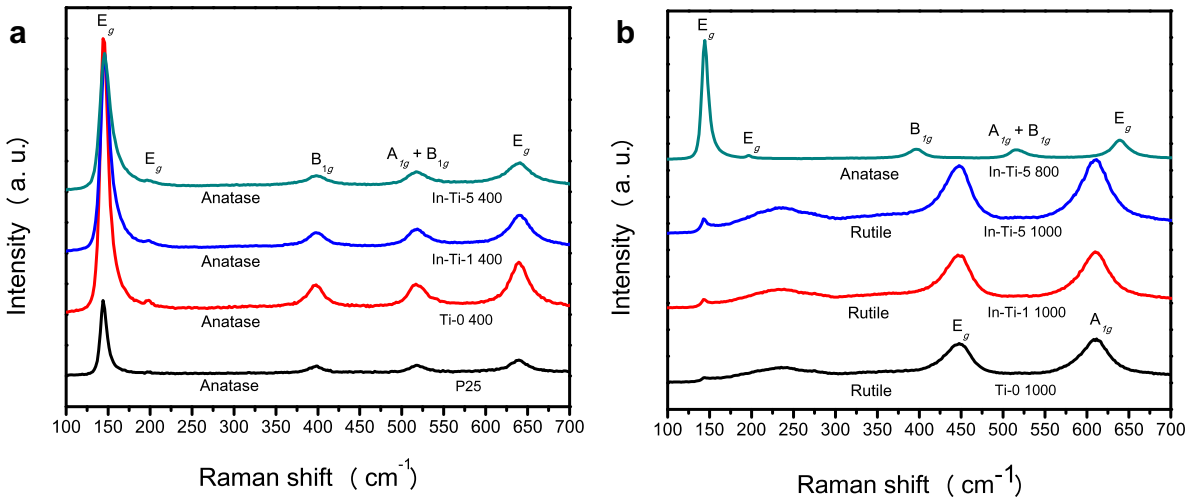

Fig. 3. Raman spectra of sol–gel semiconductors calcined: (a) at 400 °C (b) at 1000 °C.

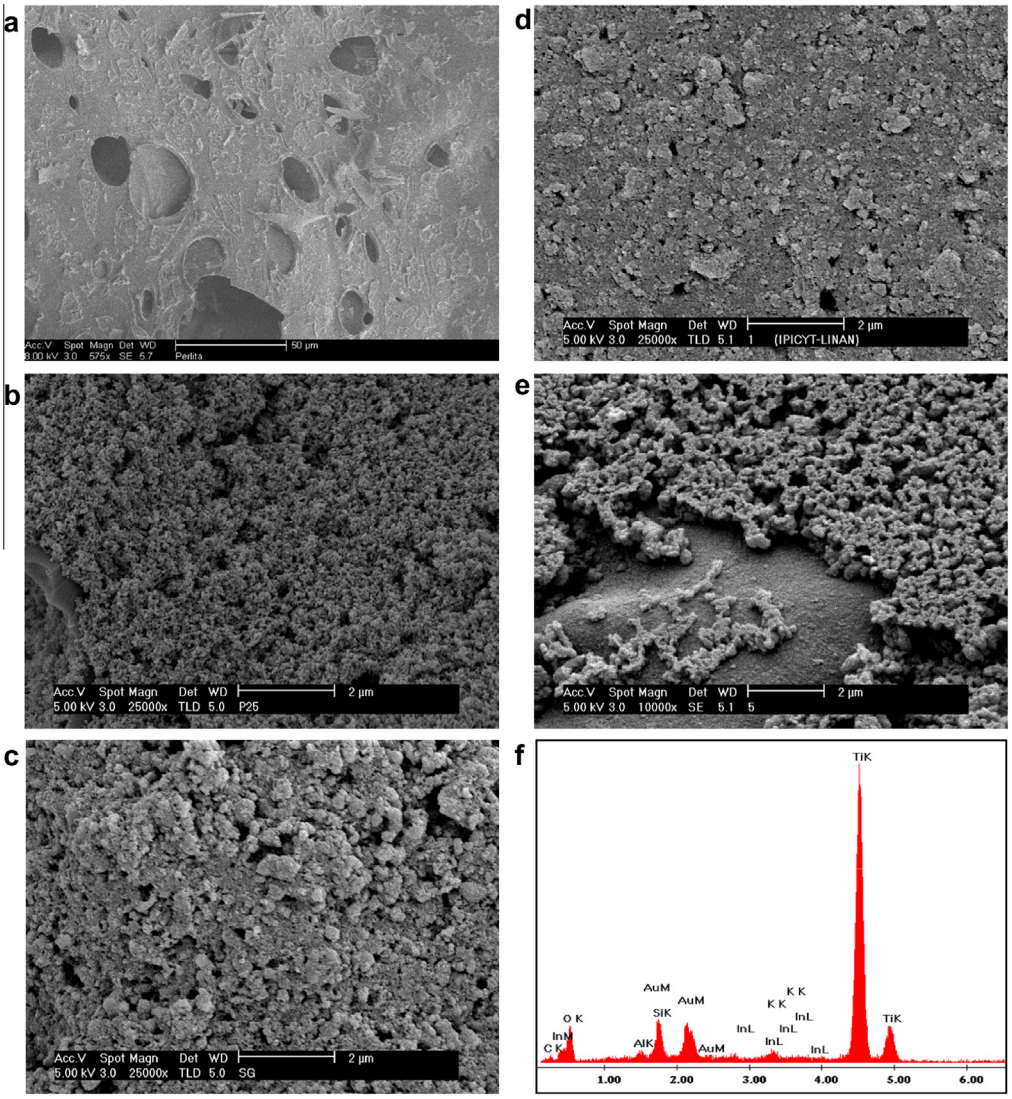

Fig. 4. SEM images for the (a) perlite, (b) P25/perlite, (c) Ti-0/perlite, (d) In–Ti-1/perlite, (e) In–Ti-5/perlite, and (f) EDS spectra of In–Ti-1/perlite.

is that Ti-0/perlite show both the highest decomposition (25.5%) and the highest DR (2.2 mol $g^{-1}s^{-1}$) than P25/perlite (16.3%, 1.4 mol $g^{-1}s^{-1}$) and In–Ti-1/perlite (19.9%, 1.3 mol $g^{-1}s^{-1}$). However, It can be seen that In–Ti-5/perlite sample show both

the highest decomposition (27.4%) and the highest DR (2.3 mol $g^{-1}s^{-1}$) also at 254 nm of UV irradiation.

These results indicate that by incorporating indium into TiO_2 the UVA photodecomposition of EB can be increased. In^{3+} ions dispersed within the TiO_2 framework may promote the breakage of bonds like C=C, C—C, and C—H, which requires energies of 596.4 kJ mol^{-1}, 336 kJ mol^{-1} and 411.6 kJ mol^{-1}, respectively [31]. A 365 nm UV lamp can break only bonds of 327.7 kJ mol^{-1} in contrast to a UV lamp at 254 nm that can break C—C and C—H bonds of 470.9 kJ mol^{-1} (photolysis). This means that the UVA decomposition of EB obtained by the photocatalysts reported here is due only to the photoactivity of coated materials.

The differences in activity and DR observed in the EB conversion over TiO_2 versus In–TiO_2 doped TiO_2 must be due to the effects of indium on the TiO_2 particles, see Fig. 5. We suggest that such effects are a consequence of the selective incorporation of the indium at Ti^{4+} and/or O^{2-} sites that perturb the formation of hexacoordinated Ti—O bonds in the TiO_2 anatase crystalline phase, thereby creating superficial defects and restricting the crystalline growth, due to stress resulting from the replacement of some oxygen atoms by In^{3+} ions. These changes are manifested in the decrease of crystallite size and the blue-shift of the band-gap energy in In–Ti-5/perlite. The adsorption may be improved with the incorporation of the indium doping into the TiO_2 as pointed out by Li et al. [6] for Ln^{3+} TiO_2 semiconductors.

The effect of the specific surface area on the photoactivity was study using at kinetic parameter, K/S_{BET}, Tables 1 and S2. This effect is in the same order for P25/perlite in both UV irradiation, 254 and 365 nm. In the case of In–Ti/perlite materials only In–Ti-5/perlite show the beneficial effect of In^{3+} ions incorporation. This material is able to decompose the EB contained in the moist air stream at the highest decomposition rate but, in terms of K/S_{BET} the presence of In_2O_3 particles on the TiO_2 surface seems to have a detrimental effect on the photocatalytic activity. However, the higher photolysis at 254 nm and the remarkable photocatalytic behavior of undoped Ti-0/perlite at 254 nm suggest that the kinetic parameter, K/S_{BET} comprises a synergic effect of photoactivity and the formation of by-products. The identification of the by-products will be carried out in all the materials to separate the synergic effect and they will be the subject of a coming communication. Finally, the evaluation of the catalyst In–Ti-1/perlite during a period of 15 days at UVA was carried out. The stability of the catalysts over time along the stream was unchanged under the same conditions, which means that the catalysts are stable during continuous photodescomposition. Considering the very low water solubility of BTEX (EB 152 mg L^{-1}), the EB and some of the by-products formed during its decomposition may to be partially dissolved in the water stream phase within the air spaces of the packed perlite granules that favor the formation of and mobility of ·OH radicals [32], mass transfer and EB reversible adsorption. Because of decomposition of EB in moist air in a plug-flow photoreactor with a concentric cylindrical configuration, the photodegradation rate of the EB may be enhanced by the TiO_2–In_2O_3 surface and optimized for In–Ti-5/perlite. As has been pointed by Skorb et al. [23] the photodegradation

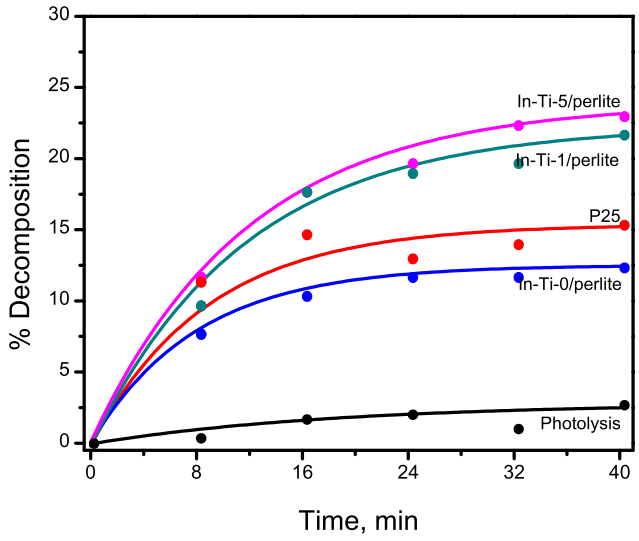

Fig. 5. Photocatalytic evolution of ethybenzene oxidation under 365 nm irradiation as a function of time.

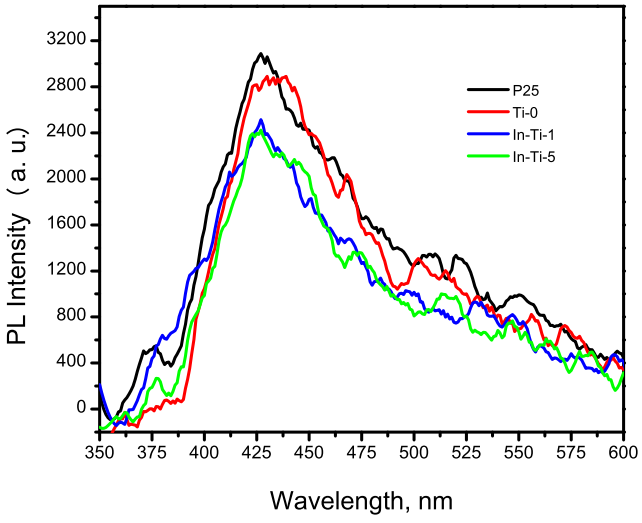

Fig. 6. PL spectra of sol–gel semiconductors calcined at 400 °C.

of polar molecules occur most rapidly at the Indium oxide titania substrate. The decomposition of EB in absence of moisture is difficult and negligible. It has been previously proposed that the incorporation of indium into the TiO_2 lattice favors the aqueous decomposition of herbicide 2,4-D [20]. When the catalyst is doped, In^{3+} on the surface of the substrate particles are created. These incorporations generate crystalline defects that are as acidic centers for indium doped Al_2O_3 used in n-heptane reformation [30]. The amount of dopant controls the level of photoactivity as well

Table 2
Photocatalytic degradation of ethylbenzene vapors at 365 nm with the catalysts P25, Ti-0, In–Ti-1, and In–Ti-5.

System	D^a (%)	Catalyst (g)	DR[a] (mol $g^{-1}s^{-1}$) 1×10^{-7}	K (s^{-1})	K/S_{BET} (gm^{-2} s^{-1}) 1×10^{-2}
Photolysis	3.3	–	–	0.5	–
P25/perlite	15.1	2.7	1.1	2.5	4.8
Ti-0/perlite	12.3	2.9	0.9	1.7	2.3
In–Ti-1/perlite	21.9	2.6	1.7	3.7	3.9
In–Ti-5/perlite	23.3	2.6	1.8	4.0	3.6

[a] D (decomposition) $D = [(C_0–C)/C_0] * 100$, DR (degradation rate), DR = (F/22400) * (PV/760) * (1000/M)*(273/T) * (%Ct/100), F (reactor flow), PV (vapor pressure), M (catalysts weight), T (temperature), %Ct (decomposition).

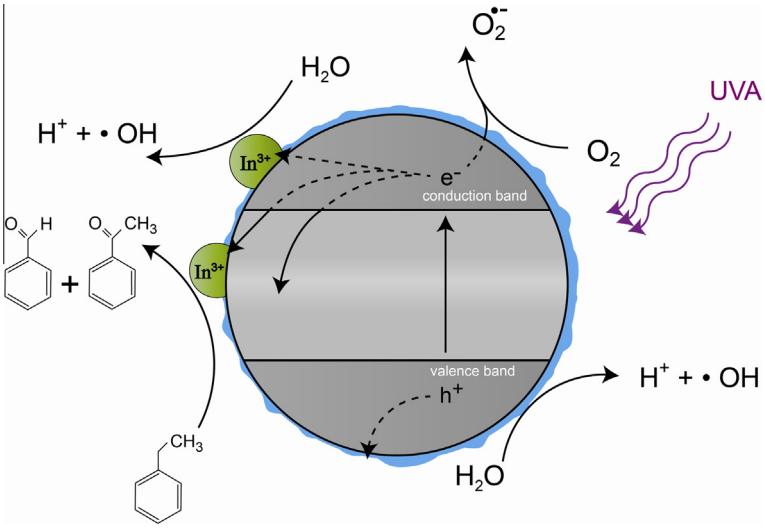

Fig. 7. Schematic representation of indium-doped TiO_2 photoexcitation.

as the crystallite size, which directly enhances the photocatalytic activity [25]. Since BTEX compounds are transported in moist air the adsorption of the hazardous organic EB molecules could exhibit reversible surface adsorption as compared to slurry systems. This weak adsorption and also the packed coated perlite promote the rapid contact of EB in an irradiated photoreactor that allows the oxidation of the contaminated material onto the indium sensitized TiO_2 photocatalysts.

Fig. 6, compares PL spectra for TiO_2 P25 and indium doped-photocatalyst, similar results were obtained for all the materials. A spectral band centered nearby 430 nm is observed, the band slightly varies in wide an intensity depending of the photocatalyst. It can be seen that TiO_2 P25 sample show the more intense band. For the catalysts with Indium the intensity gradually decrease, showing the slightly intensity of band the In–Ti-5 photocatalyst. Photo-excitation causes electrons within the material to move into permissible excited states. When these electrons return to their equilibrium states, the excess energy is unconfined and could include the emission of light. It seems that the indium incorporation suppress the electron–hole recombination at the photocatalyst surface and leads to increase the transfer to photo-generated electrons, requiring less light absorption for photo-excitation. In the literature was propose that the spectral PL band centered nearby 420 nm is associated with oxygen vacancies created during the doping of TiO_2 [34].

The schematic representation of indium-doped TiO_2 photoexcitation, Fig. 7, was made according to model evaluation of the photocatalysts on aqueous phenol degradation and PL results (see supplementary material). It is suggested that P25 acts via hydroxyl radicals ($OH^{\cdot}$) during the gas-phase photocatalytic decomposition of ethylbenzene, producing probably more intermediates [35]. In the case of indium doped TiO_2, the photoactivity is enhanced due to improved charge separation and direct ethylbenzene oxidation at the sites of the indium doping at the surface of these materials. The mineralization of EB was incomplete due to the high initial concentration of EB in the gas phase. Some volatile intermediate compounds of the irradiated gas stream were identified by GC–MS [34], principally as benzaldehyde, acetophenone. These photoproduct intermediaries are formed by direct photo-oxygenation of organic radicals of EB [33].

The concentration of EB used in this study may also be encountered at commercial gasoline stations. Lastly, we combined to couple these photocatalytic processes with a biofiltration process in order to achieve greater EB removal. Interestingly, this hybrid process provides 36% of additional removal of EB in 16 days. However, the presence of the biofilter does not guarantee the mineralization of EB [36].

4. Conclusions

The incorporation of In^{3+} into TiO_2 frameworks restricts the formation of hexacoordinated titanium and also creates oxygen vacancies and defects that act as discrete reactive sites. The FE-SEM images, as well as the EDS analysis, confirm that TiO_2 and indium-doped TiO_2 homogenous coating is achieved successfully after a 60 min. The incorporation of indium improved surface area that enhances adsorption of EB and rapid decomposition of its photoproducts. It is shown that in the photocatalytic decomposition rate of EB in gas-phase strongly depends on the content of indium oxide incorporated into TiO_2. The coatings with 5% content of indium show an enhanced decomposition rate in contrast to the undoped materials. It seems that indium incorporation can enhance photodecomposition under UVA in contrast to UVB, so they can acts as UVA light sensitive photocatalyst.

This research offers a low-cost method for the immobilization of indium doped TiO_2 catalysts, prepared by sol–gel coating on perlite granules that allows for the efficient moist air decomposition of EB in indoor or outdoor environments.

Acknowledgments

M.H.R. thanks CONACYT for fellowship. We thank Dr. H.C. Rosu for a careful reading of the text. The use of the infrastructure of LINAN and LANBAMA are also gratefully acknowledged. We thank M.C.D. Partida-Gutiérrez, M.C.G. Vidriales-Escobar, M.C.G. Labrada-Delgado and M.C.B. Rivera-Escoto for their technical assistance.

Appendix A. Supplementary material

Supplementary data associated with this article can be found, in the online version, at http://dx.doi.org/10.1016/j.cej.2013.01.066.

References

[1] US EPA (United States Environmental Protection Agency). Data from the National Emissions Inventory, Version 2.0, 2009. <http://www.epa.gov/ttn/chief/eiinformation.html> (accessed 2009).

[2] S. Wang, H.M. Ang, M.O. Tade, Volatile organic compounds in indoor environment and photocatalytic oxidation: state of the art, Environ. Int. 33 (2007) 694–705.
[3] US Environmental Protection Agency. Integrated Risk Information System (IRIS) on Ethylbenzene National Center for Environmental Assessment, Office of Research and Development, Washington, DC, 1999.
[4] A. Vidal, J. Herrero, M. Romero, B. Sánchez, M. Sánchez, Heterogeneous photocatalysis: degradation of ethylbenzene in TiO_2 aqueous suspensions, J. Photochem. Photobiol. A 79 (1994) 213–219.
[5] K. Kabra, R. Chaudhary, R.L. Sawhney, Treatment of hazardous organic and inorganic compounds through aqueous-phase photocatalysis: a review, Ind. Eng. Chem. Res. 43 (2004) 7683–7696.
[6] F.B. Li, X.Z. Li, C.H. Ao, S.C. Lee, M.F. Hou, Enhanced photocatalytic degradation of VOCs using Ln^{3+}–TiO_2 catalysts for indoor air purification, Chemosphere 59 (2005) 787–800.
[7] R. Vinu, G. Madras, Environmental remediation by photocatalysis, J. Indian I. Sci. 90 (2010) 189–230.
[8] A.L. Linsebigler, G. Lu, J.T. Yates, Photocatalysis on TiO_2 surfaces: principles, mechanisms, and selected results, Chem. Rev. 95 (1995) 735–758.
[9] M.R. Hoffmann, S.T. Martin, W. Choi, D.W. Bahnemann, Environmental applications of semiconductor photocatalysis, Chem. Rev. 95 (1995) 69–96.
[10] S.N. Hosseini, S.M. Borghei, M. Vossoughi, N. Tagavinia, Immobilization of TiO_2 on perlite granules for photocatalytic degradation of phenol, Appl. Catal. B 74 (2007) 53–62.
[11] M. Faramarzpour, M. Vossoughi, M. Borghei, Photocatalytic degradation of furfural by titania nanoparticles in a floating-bed photoreactor, Chem. Eng. J. 146 (2009) 79–85.
[12] A. Strini, S. Cassese, L. Schiavi, Measurement of benzene, toluene, ethylbenzene and *o*-xylene gas phase photodegradation by titanium dioxide dispersed in cementitious materials using a mixed flow reactor, Appl. Catal. B 61 (2005) 90–97.
[13] W.K. Jo, K.H. Park, Heterogeneous photocatalysis of aromatic and chlorinated volatile organic compounds (VOCs) for non-occupational indoor air application, Chemosphere 57 (2004) 555–565.
[14] S. Obregón-Alfaro, V. Rodríguez-González, A.A. Zaldívar-Cadena, S.W. Lee, Sonochemical deposition of silver–TiO_2 nanocomposites onto foamed waste-glass: evaluation of Eosin Y decomposition under sunlight irradiation, Catal. Today 166 (2011) 166–171.
[15] G. Vijayakumar, M. Dharmendirakumar, S. Renganathan, S. Sivanesan, G. Baskar, K.P. Elango, Removal of congo red from aqueous solutions by perlite, Clean 37 (2009) 355–364.
[16] M. Dogan, M. Alkan, Removal of methyl violet from aqueous solution by perlite, J. Colloid Interf. Sci. 267 (2003) 32–41.
[17] Y. Na, S. Song, Y. Park, Photocatalytic decolorization of rhodamine B by immobilized TiO_2/UV in a fluidized-bed reactor, Korean J. Chem. Eng. 22 (2005) 196–200.
[18] X.Z. Wang, Q.Q. Gao, H.T. Zhao, K. Feng, R. Guo, Synthesis of nano TiO_2/CTMAB-expanded perlite applied to the degradation of methyl orange, Appl. Mech. Mater. 110–116 (2011) 3801–3806.
[19] C.A. Korologos, C.J. Philippopoulos, S.G. Poulopoulos, The effect of water presence on the photocatalytic oxidation of benzene, toluene, ethylbenzene and mxylene in the gas-phase, Atmos. Environ. 45 (2011) 7089–7095.
[20] V. Rodríguez-González, A. Moreno-Rodríguez, M. May, F. Tzompantzi, R. Gómez, Slurry photodegradation of 2,4-dichlorophenoxyacetic acid: a comparative study of impregnated and sol–gel In_2O_3–TiO_2 mixed oxide catalysts, J. Photochem. Photobiol. A 193 (2008) 266–270.
[21] V. Stengl, F. Oplustil, T. Nemec, In^{3+}-doped TiO_2 and TiO_2/In_2S_3 nanocomposite for photocatalytic stoichiometric degradations, Photochem. Photobiol. 88 (2012) 265–276.
[22] D. Shchukin, S. Poznyak, A. Kulak, P. Pichat, TiO_2–In_2O_3 photocatalysts: preparation, characterizations and activity for 2-chlorophenol degradation in water, J. Photochem. Photobiol. A 162 (2004) 423–430.
[23] E.V. Skorb, E.A. Ustinovich, A.I. Kulak, D.V. Sviridov, Photocatalytic activity of TiO_2:In_2O_3 nanocomposite films towards the degradation of arylmethane and azo dyes, J. Photochem. Photobiol. A 193 (2008) 97–102.
[24] E.V. Skorb, L.I. Antonouskaya, N.A. Belyasova, D.G. Shchukin, H. Möhwald, D.V. Sviridov, Antibacterial activity of thin-film photocatalysts based on metal-modified TiO_2 and TiO_2:In_2O_3 nanocomposite, Appl. Catal. B 84 (2008) 94–99.
[25] V. Rodríguez-González, F. Paraguay-Delgado, X. García-Montelongo, L.M. Torres-Martínez, R. Gómez, Effect of the In_2O_3 content on the photodegradation of the alizarin dye using TiO_2–In_2O_3 nanostructured semiconductors, J. Ceram. Process. Res. 9 (2008) 606–610.
[26] Y. Chen, X. Zhou, X. Zhao, X. He, X. Gu, Crystallite structure, surface morphology and optical properties of In_2O_3–TiO_2 composite thin films by sol–gel method, Mater. Sci. Eng., B 151 (2008) 179–186.
[27] M.A. Debeila, R.P.K. Wells, J.A. Anderson, Influence of water and pretreatment conditions on CO oxidation over Au/TiO_2–In_2O_3 catalysts, J. Catal. 239 (2006) 162–172.
[28] C. Liang, G. Meng, Y. Lei, F. Phillipp, L. Zhang, Catalytic growth of semiconducting In_2O_3 nanofibers, Adv. Mater. 13 (2001) 1330–1333.
[29] S.K. Poznyak, D.V. Talapin, A.I. Kulak, Structural, optical, and photoelectrochemical properties of nanocrystalline TiO_2–In_2O_3 composite solids and films prepared by sol–gel method, J. Phys. Chem. B 105 (2001) 4816–4823.
[30] V. Rodríguez-González, R. Gómez, M. Moscosa-Santillan, J. Amouroux, Synthesis, characterization, and catalytic activity in the n-heptane conversion over Pt/In–Al_2O_3 sol-gel prepared catalysts, J. Sol–Gel Sci. Techn. 42 (2007) 165–171.
[31] Z.-W. Cheng, Y.-F. Jiang, L.-L. Zhang, J.-M. Chen, Y.-Y. Wei, Conversion characteristics and kinetic analysis of gaseous α-pinene degradaded by a VUV light in various reaction media, Sep. Purif. Technol. 77 (2011) 26–32.
[32] P. Pichat, Some views about indoor air photocatalytic treatment using TiO_2: conceptualization of humidity effects, active oxygen species, problem of C1–C3 carbonyl pollutants, Appl. Catal. B 99 (2010) 428–434.
[33] Thomas Oppenländer, Photochemical and Purification of Water and Air, Wiley-VCH, Alemania, 2003.
[34] N. Serpone, Is the band gap of pristine TiO_2 narrowed by anion- and cation-doping of titanium dioxide in second-generation photocatalysts, J. Phys. Chem. B 110 (2006) 24287–24293.
[35] A. Sobczynski, L. Duczmal, W. Zmudzinski, Phenol destruction by photocatalysis on TiO_2: an attempt to solve the reaction mechanism, J. Mol. Catal. A – Chem 213 (2004) 225–230.
[36] M. Hinojosa-Reyes, V. Rodríguez-González, S. Arriaga, Enhancing ethylbenzene vapors degradation in a hybrid system based on photocatalytic oxidation UV/TiO_2–In and a biofiltration process, J. Hazar. Mater. 209 (2012) 365–371.